Semimetallic behavior in Heusler-type Ru_2TaAl and thermoelectric performance improved by off-stoichiometry

C. W. Tseng,[1] C. N. Kuo,[1] H. W. Lee,[2] K. F. Chen,[1] R. C. Huang,[3] C.-M. Wei,[2] Y. K. Kuo,[3,*] and C. S. Lue[1,†]

[1]*Department of Physics, National Cheng Kung University, Tainan 70101, Taiwan*

[2]*Institute of Atomic and Molecular Sciences, Academia Sinica, Taipei 10617, Taiwan*

[3]*Department of Physics, National Dong Hwa University, Hualien 97401, Taiwan*

(Received 7 June 2017; revised manuscript received 24 August 2017; published 5 September 2017)

We report a study of the temperature-dependent electrical resistivity, Seebeck coefficient, thermal conductivity, specific heat, and ^{27}Al nuclear magnetic resonance (NMR) in Heusler-type Ru_2TaAl, to shed light on its semimetallic behavior. While the temperature dependence of the electrical resistivity exhibits semiconductorlike behavior, the analysis of low-temperature specific heat reveals a residual Fermi-level density of states (DOS). Both observations can be realized by means of a semimetallic scenario with the Fermi energy located in the pseudogap of the electronic DOS. The NMR Knight shift and spin-lattice relaxation rate show activated behavior at higher temperatures, attributing to the thermally excited carriers across a pseudogap in Ru_2TaAl. From the first-principles band structure calculations, we further provide a clear picture that an indirect overlap between electron and hole pockets is responsible for the formation of a pseudogap in the vicinity of the Fermi level of Ru_2TaAl. In addition, an effort for improving the thermoelectric performance of Ru_2TaAl has been made by investigating the thermoelectric properties of $Ru_{1.95}Ta_{1.05}Al$. We found significant enhancements in the electrical conductivity and Seebeck coefficient and marked reduction in the thermal conductivity via the off-stoichiometric approach. This leads to an increase in the figure-of-merit ZT value from 6.1×10^{-4} in Ru_2TaAl to 3.4×10^{-3} in $Ru_{1.95}Ta_{1.05}Al$ at room temperature. In this respect, a further improvement of thermoelectric performance based on Ru_2TaAl through other off-stoichiometric attempts is highly probable.

DOI: 10.1103/PhysRevB.96.125106

I. INTRODUCTION

Heusler-type intermetallics with cubic $L2_1$ (Cu_2MnAl-type) structure have attracted considerable attention because of their various magnetic and transport features [1]. The variety of physical properties are highly associated with the nature of hybridization between the orbitals of the constituent atoms. In principle, the number of valence electrons per formula unit (VE) plays an important role for the modification of the electronic structure near the Fermi level (E_F) [2]. Accordingly, nonmagnetic semiconductors or semimetals are anticipated for the Heusler compounds with VE = 24. The iron-based members such as Fe_2VAl, Fe_2VGa, and Fe_2TiSn have been classified as the materials within this prototype [3–11]. The electronic density of states (DOS) of each individual compound features a narrow pseudogap at around E_F which is promising for developing efficient thermoelectrics. As a matter of fact, the Fe_2VAl related compounds have been widely studied for improving the thermoelectric figure of merit (ZT) through various attempts [12–21].

Intermetallic Ru_2TaAl belongs to the family of Heusler compounds with VE = 24 [22]. Nevertheless, its physical properties remain unexplored. In this work, we performed a detailed study of Ru_2TaAl by means of the electrical resistivity (ρ), Seebeck coefficient (S), thermal conductivity (κ), specific heat (C_P), as well as ^{27}Al nuclear magnetic resonance (NMR) measurements to shed light on its electronic properties, essentially for the realization of the pseudogap feature near E_F. All observations are consistent with semimetallic characteristics in Ru_2TaAl. We have also carried out the electronic structure calculations and the calculated result reveals an indirect overlap between electron and hole pockets that gives rise to a pseudogap in the vicinity of E_F. Such a scenario provides a reasonable interpretation for the semimetallic behavior in Ru_2TaAl established from the present investigation. To improve the thermoelectric performance of Ru_2TaAl, we have studied the thermoelectric properties on the off-stoichiometric $Ru_{1.95}Ta_{1.05}Al$ compound. We found a marked reduction in the thermal conductivity along with enhanced Seebeck coefficient and electrical conductivity which lead to a significant enhancement in the ZT value, about six times larger than that of stoichiometric Ru_2TaAl at room temperature.

II. EXPERIMENTAL RESULTS AND DISCUSSION

Ru_2TaAl and $Ru_{1.95}Ta_{1.05}Al$ ingots were prepared by an ordinary arc-melting technique. Briefly, the mixture of 99.9% Ru, 99.9% Ta, and 99.99% Al elemental metals with the corresponding ratio was placed in a water-cooled copper hearth and then melted several times in an argon flow arc melter. To promote homogeneity, the as-cast samples were annealed in a vacuum-sealed quartz tube at 800 °C for 2 days, and then at 400 °C for more than 12 h followed by furnace cooling. This is a typical process to form a single-phase Heusler compound [3,12–14,23–25]. A room-temperature x-ray diffraction taken with Cu $K\alpha$ radiation on the powdered Ru_2TaAl specimen is shown in Fig. 1. All diffraction peaks were indexed to the $L2_1$ structure (space group $Fm\bar{3}m$). We determined the lattice constant $a = 6.13$ Å for Ru_2TaAl, being consistent with the value reported in the literature [26].

*ykkuo@mail.ndhu.edu.tw

†cslue@mail.ncku.edu.tw

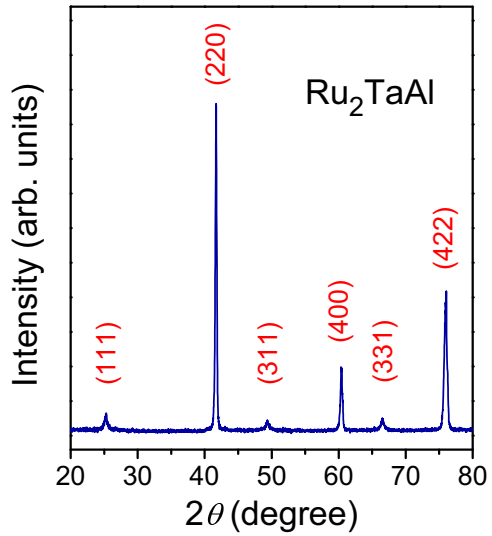

FIG. 1. X-ray diffraction pattern for the powdered Ru_2TaAl. Reflections are indexed with respect to the Cu_2MnAl-type $L2_1$ structure.

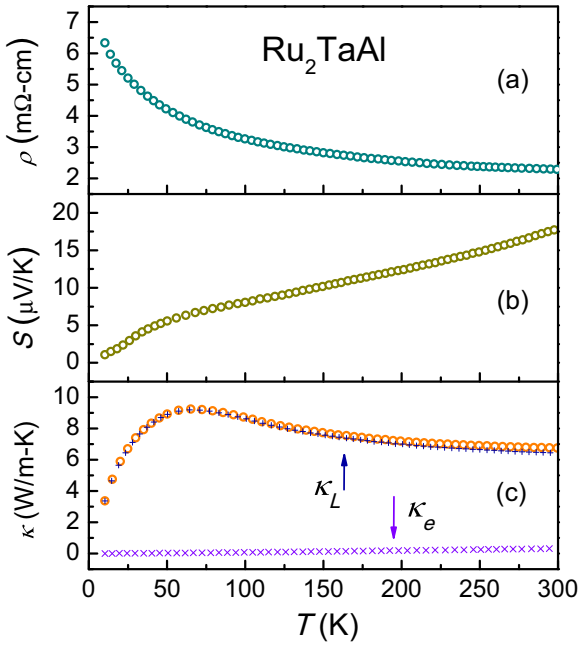

FIG. 2. (a) Electrical resistivity ρ as a function of temperature for Ru_2TaAl. (b) Temperature dependence of the Seebeck coefficient S for Ru_2TaAl. (c) Temperature variations of the total thermal conductivity κ, lattice thermal conductivity κ_L, and electronic thermal conductivity κ_e for Ru_2TaAl.

It should be noted that the presence of antisite disorder is often found in the Heusler-type X_2YZ compounds [27]. In principle, the presence of antisite disorder between Y and Z atoms would lead to a diminished (111) peak toward $B2$-type structure. For the present case of Ru_2TaAl, the (111) diffraction peak is clearly seen, indicating little or no effect of $B2$-type disorder. On the other hand, the (200) diffraction peak is invisible in our Ru_2TaAl. We associate this observation with almost equal scattering factors of Ru, Ta, and Al in Ru_2TaAl, leading to vanishing the (200) peak.

A. Electrical transport and thermoelectric properties

In Fig. 2(a) we show the temperature variation of the electrical resistivity $\rho(T)$ for Ru_2TaAl. It clearly exhibits nonmetallic behavior as indicated by its negative temperature coefficient of resistivity, i.e., it decreases with increasing temperature with a value of about 2.3 mΩ cm at room temperature. Due to its finite residual resistivity at low temperatures, this material should be classified as a semimetal. Similar $\rho(T)$ features have been found in other ruthenium-based semimetallic Heusler compounds such as Ru_2NbGa [28]. The activated transport behavior observed in Ru_2TaAl can be realized as the thermally excited carriers across the pseudogap near E_F, in analogy to the case of Ru_2NbGa.

The T-dependent Seebeck coefficient $S(T)$ of Ru_2TaAl is displayed in Fig. 2(b), with a magnitude of about 18 μV/K at room temperature. The positive sign of S suggests that the hole-type carriers dominate the thermoelectric transport of Ru_2TaAl. The measured T-dependent total thermal conductivity $\kappa(T)$ of Ru_2TaAl is given in Fig. 2(c). It is remarkable that the value of κ at room temperature is only 6.7 W/mK, much lower than that in Fe_2VAl ($\sim$25 W/mK). This is presumably due to the heavier Ru and Ta atoms in place of Fe and V, making the heat conduction by long wavelength phonon modes less effective in Ru_2TaAl. In this respect, the inherent low κ in Ru_2TaAl makes it a potential candidate for thermoelectric applications. In metals and semimetals, thermal conductivity is a sum of the lattice component and the electronic component (κ_e), i.e., $\kappa(T) = \kappa_L(T) + \kappa_e(T)$. Here, $\kappa_L(T)$ was obtained by subtracting the measured $\kappa(T)$ with $\kappa_e(T)$ that can be evaluated by the Wiedemann-Franz law: $\kappa_e\rho/T = L_0$, where ρ is the measured dc electric resistivity and $L_0 = 2.45 \times 10^{-8}$ W Ω K^{-2} is the Lorenz number. From this estimation, it yields a minor contribution from κ_e, indicating that the observed thermal conductivity of Ru_2TaAl is dominated by κ_L.

In order to improve ZT in Ru_2TaAl, we have studied the thermoelectric properties on the off-stoichiometric compound $Ru_{1.95}Ta_{1.05}Al$. The obtained T-dependent $\rho(T)$ for $Ru_{1.95}Ta_{1.05}Al$ is shown in Fig. 3(a). It is noted that the magnitude of ρ reduces to $\sim$1.8 mΩ cm at room temperature, while it still exhibits a semiconductinglike behavior. For the T-dependent $S(T)$ of $Ru_{1.95}Ta_{1.05}Al$, it shows a sign change to negative as illustrated in Fig. 3(b), suggesting that the electrons become dominant for the thermoelectric transport of $Ru_{1.95}Ta_{1.05}Al$. A similar sign reversal in S has also been reported in the isostructural $Fe_{2-x}V_{1+x}Al$ system [13,29,30]. From previous various investigations [31–37], the replacement of Fe by V in Fe_2VAl may cause the modification of electronic structure, the presence of the impurity state within the pseudogap, and/or the accompanying other disorder effects. Those would play different roles on the type of carriers and thus lead to the sign change in S. Based on the similarity between Ru_2TaAl and Fe_2VAl, it is realistic to associate the observed sign reversal in S of $Ru_{1.95}Ta_{1.05}Al$ with similar origins.

While interpreting the sign reversal in S may be complicated by the combination of various effects, it is unambiguous

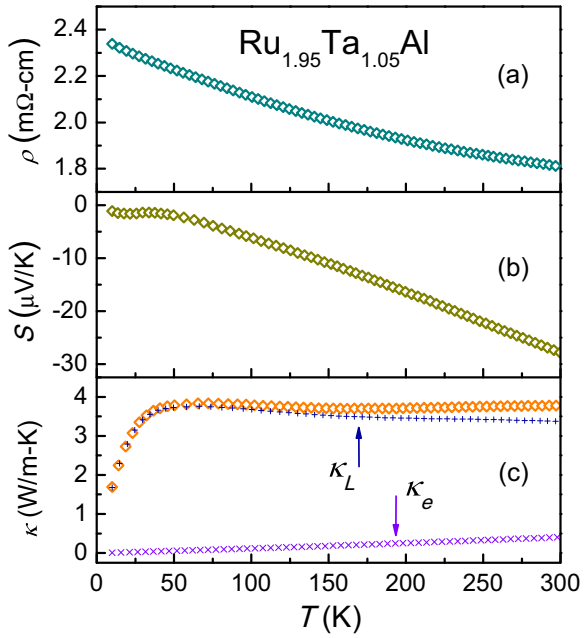

FIG. 3. (a) Electrical resistivity ρ as a function of temperature for $Ru_{1.95}Ta_{1.05}Al$. (b) Temperature dependence of the Seebeck coefficient S for $Ru_{1.95}Ta_{1.05}Al$. (c) Temperature variations of κ, κ_L, and κ_e for $Ru_{1.95}Ta_{1.05}Al$.

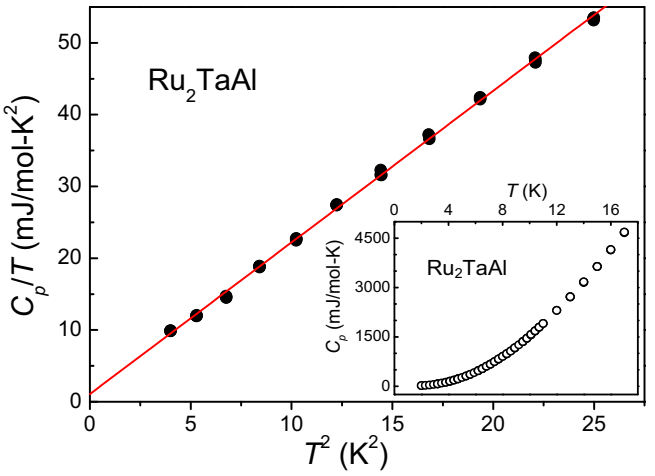

FIG. 4. A plot of C_p/T versus T^2 for Ru_2TaAl. The solid line is a fit to the experimental data according to $C_p/T = \gamma + \beta T^2$. Inset: Temperature dependence of the specific heat for Ru_2TaAl.

for the observation of an enhancement in the absolute value of S, showing an increasing magnitude to ~ 28 μV/K at room temperature in $Ru_{1.95}Ta_{1.05}Al$. As compared to Fe_2VAl, the absolute value of S greater than 100 μV/K at room temperature has been obtained in the off-stoichiometric $Fe_{2-x}V_{1+x}Al$ ($0.02 < x < 0.08$) and $Fe_{2.02}V_{1.01}Al_{0.97}$ compounds [12,13,29,30]. It thus suggests that a further improvement of S in Ru_2TaAl should be achieved through similar off-stoichiometric approaches.

In general, the major difficulty in obtaining good thermoelectric performance of materials is to enhance the power factor ($PF = S^2/\rho$) while simultaneously reducing κ [38–41]. For $Ru_{1.95}Ta_{1.05}Al$, we found that the room-temperature κ is suppressed to about 3.8 W/mK, as indicated in Fig. 3(c). As a result, the considerably low κ along with an enhanced PF lead to a substantial enhancement in the room-temperature ZT from Ru_2TaAl ($\sim 6.1 \times 10^{-4}$) to $Ru_{1.95}Ta_{1.05}Al$ ($\sim 3.4 \times 10^{-3}$). Although the current ZT value is still lower than that of the state-of-the-art thermoelectric materials, further improvement in ZT by incorporating antisite disorder or by doping various elements in different crystallographic sites should be highly anticipated [12–21,42–44].

B. Low-temperature specific heat

The low-temperature specific heat C_p measurement was performed using a ^{3}He heat-pulsed thermal relaxation calorimeter in the temperature range from 1.8 to 16 K with the result shown in the inset of Fig. 4. The analysis of the specific heat data allows the determination of the Sommerfeld constant γ and Debye constant β from $C_p(T) = \gamma T + \beta T^3$. We thus displayed the plot of C_p/T vs T^2 in Fig. 4, with a solid line representing the best fit to the experimental data. Such a fit yields $\gamma = 1.07$ mJ/mol K^2 and $\beta = 2.11$ mJ/mol K^4 for Ru_2TaAl. The Debye temperature θ_D of 155 K can be evaluated from β using the relation $\theta_D = (12\pi^4 RZ/5\beta)^{1/3}$, where $R = 8.314$ J/mol K is the molar gas constant and $Z = 4$ is the number of atoms per unit cell.

It is noticed that the magnitude of γ for Ru_2TaAl is rather small, much lower than the values of 10–20 mJ/mol K^2 reported for metallic Heusler compounds such as Ni_2HfAl and Ni_2ZrGa [45,46]. With this comparison, it implies a small electronic DOS near E_F for Ru_2TaAl. Within the free electron gas model, the Fermi-level DOS $N(E_F)$ can be estimated according to the relation

$$\gamma = \frac{\pi^2 k_B^2}{3} N(E_F). \quad (1)$$

We thus extracted $N(E_F) = 0.45$ states/eV f.u. which is a bit lower than the value of about 0.6 states/eV f.u. in semimetallic Fe_2VAl [5]. In this respect, it reinforces the conclusion that Ru_2TaAl should be characterized as a semimetal.

C. ^{27}Al nuclear magnetic resonance

Nuclear magnetic resonance is known as a local probe yielding information about Fermi surface features. In this study, we have carried out the ^{27}Al NMR measurements on powdered Ru_2TaAl specimens under a constant field of 7.08 T. Central transition line shapes were obtained from spin echo fast Fourier transforms using a standard $\pi/2$-τ-π sequence. Several representative spectra taken at various temperatures are given in the inset of Fig. 5. The ^{27}Al NMR Knight shift ^{27}K is determined from the position of the maximum of each spectrum with respect to an aqueous $AlCl_3$. The T-dependent ^{27}K of Ru_2TaAl is illustrated in Fig. 5. We found that ^{27}K remains almost T independent at low temperatures with a small magnitude of about 0.035%. This is consistent with a semimetallic material with a low residual DOS at E_F. Above 280 K, ^{27}K shifts to higher frequency with rising temperature, reflecting an increase in the spin susceptibility,

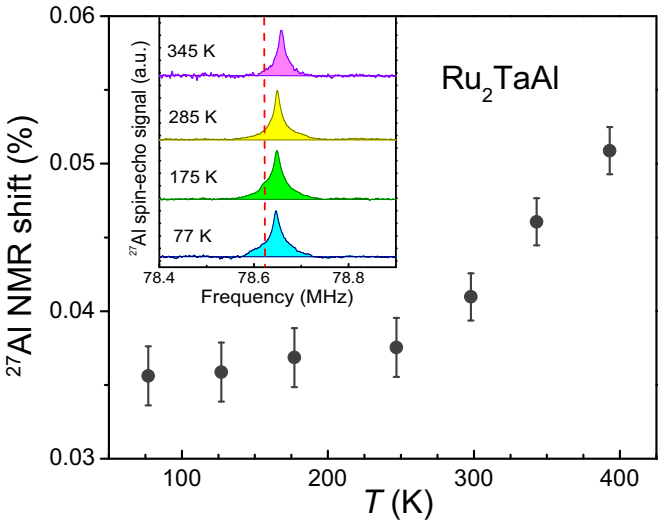

FIG. 5. Temperature dependence of the ^{27}Al NMR Knight shift ^{27}K for Ru_2TaAl. Inset: Representative ^{27}Al NMR central transition spectra measured at various temperatures. The dashed vertical line denotes the position of the ^{27}Al reference frequency.

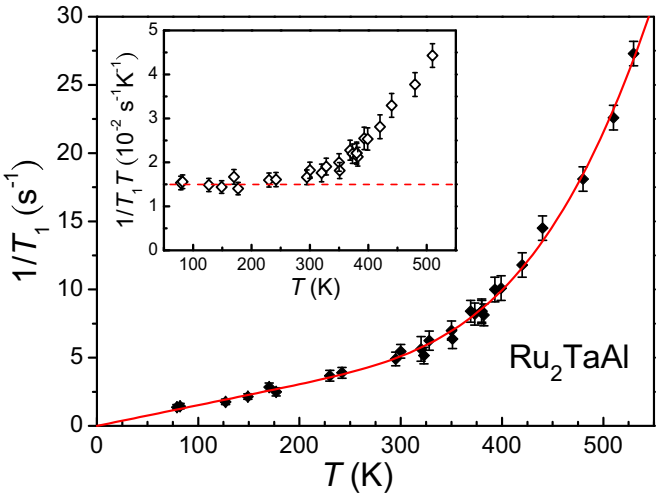

FIG. 6. Temperature dependence of the ^{27}Al spin-lattice relaxation rate $1/T_1$ for Ru_2TaAl. The solid curve is a fit to the Korringa relation plus thermally activated behavior described in the text.

attributed to a thermally activated increase in the number of carriers, also responsible for the enhancement in the relaxation rate. Contrary to other gapped systems such as Fe_2VAl and Fe_2VGa [4,7], the ^{51}V Knight shifts were found to shift to lower frequencies with temperature, owing to the negative core polarization of vanadium d states. Rather, the thermally excited carriers in Ru_2TaAl are mainly s character because of the positive $s-$hyperfine constant. These carriers are responsible for the T-dependent Knight shift and spin-lattice relaxation rate at elevated temperatures. It is worthwhile mentioning that similar responses have been observed in the ^{59}Co NMR measurements on the semiconducting and semimetallic Co-based skutterudites [47,48].

The ^{27}Al NMR spin-lattice relaxation rate $1/T_1$ was obtained by integrating the spin echo signal using the inversion recovery method. To further examine the pseudogap feature, the $1/T_1$ measurement was extended to 540 K. The temperature dependence of ^{27}Al $1/T_1$ for Ru_2TaAl is displayed in Fig. 6, showing a linear increase upon heating and then a rapid rise above 280 K. In the inset of Fig. 6, we plot $1/T_1T$ vs T for demonstrating a pronounced increase beyond the Korringa relation (constant $1/T_1T$) [49]. Similar features have been found in ^{27}Al $1/T_1$ of semimetallic $CaAl_2Si_2$, $SrAl_2Si_2$, and $RuAl_2$ [50–52]. By analogy, the T-dependent $1/T_1$ of Ru_2TaAl can be expressed by $CT + AT^2\exp(-E_A/2k_BT)$, where C, A, and E_A are fitting parameters. The first term is due to the Korringa relation arising from the relaxation process of the conduction electrons, and the second is characterized by the additional contribution via thermally excited carriers across an activation energy E_A. The band dispersion here was approximated by the square root of the energy near each band edge. The corresponding carrier density of the conduction electrons varies with temperature according to $T^{3/2}\exp(-E_A/2k_BT)$. The optimum fit with $C = 1.5 \pm 0.4 \times 10^{-3}$ s^{-1}K^{-1}, $A = 1.6 \pm 0.4 \times 10^{-3}$ s^{-1}K^{-2}, and $E_A = 0.29 \pm 0.02$ eV, is shown as a solid curve over the entire temperature range in Fig. 6. It is remarkable that the extracted E_A of about 0.29 eV is quite close to the magnitude of the pseudogap obtained from theoretical electronic structure calculations which will be described in the following section. With this accordance, we have a concise picture that the activated behavior in ^{27}Al$1/T_1$ could be attributed to the thermally excited carriers across the pseudogap in Ru_2TaAl.

The Korringa process for the relaxation of Al nuclear spins in Ru_2TaAl is dominated by the Al 3s electrons and can be expressed as [49]

$$\frac{1}{T_1T} = 2hk_B\left[{}^{27}\gamma_n H_{hf}^s N_s(E_F)\right]^2. \quad (2)$$

Here $^{27}\gamma_n$ is the Al nuclear gyromagnetic ratio, H_{hf}^s is the hyperfine field per spin of the Al s electrons, and $N_s(E_F)$ is the Al 3s Fermi-level DOS in units of states/eV per spin. Taking $H_{hf}^s \sim 1.9 \times 10^6$ G for Al metal [50,51,53–56], the experimental value of $C = 1.5 \times 10^{-3}$ s^{-1}K^{-1} would yield $N_s(E_F) = 0.007$ states/eV f.u. Note that this value is an order of magnitude smaller than those in Al-based metals, supporting the scenario of the semimetallic nature for Ru_2TaAl.

D. Electronic structure calculations

In this section, we have tried to gain further insight into the electronic band structure of Ru_2TaAl from the perspective of first principles; however, it is known that the most common first-principles method, density functional theory (DFT), has drawbacks stemming from its exchange-correlation approximations in the electronic many-body effect, and thus might yield to unreasonable or unreliable band structures. Whereas, the GW methods [57], by calculating dynamically screened Coulomb interaction (W) and Green's functions (G), have included the many-body interaction and thus will produce reliable band structures. Taking our previous studies related

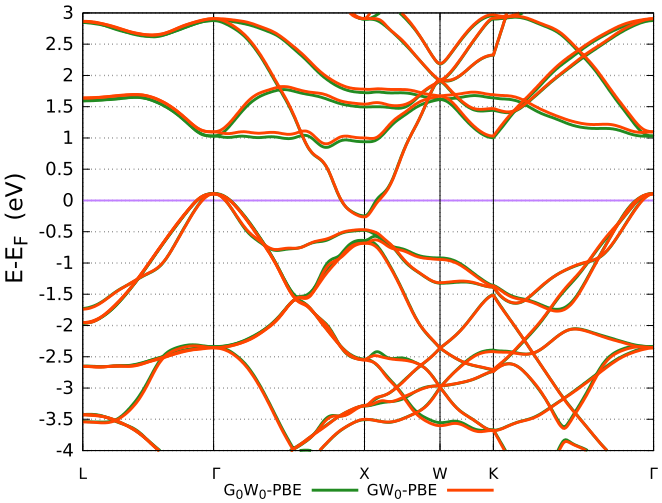

FIG. 7. G_0W_0 and GW_0 band structures using PBE initial wave functions for Ru_2TaAl. The zero of energy is placed at the Fermi level.

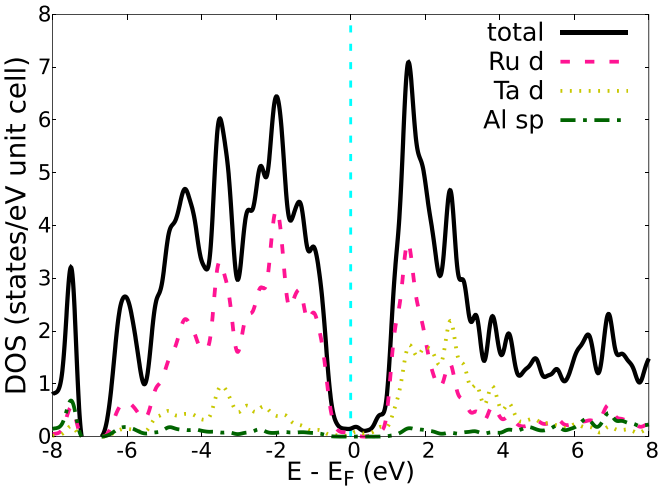

FIG. 8. The GW_0-PBE total and site-decomposed density of states of Ru_2TaAl. The Fermi level is set at zero.

to Ru_2NbGa as an example [28], the band structures obtained from DFT frameworks [Perdew-Burke-Ernzerhof (PBE) and HSE06) [58,59] are controversial while the results obtained from the GW_0 approximation [60] using either PBE or HSE06 initial wave functions have yielded consistent and reliable band structures. Based on the previous work [28], we have performed the first-principles total-energy calculations with GW_0 or G_0W_0 corrections [60,61] for the band gaps using PBE initial wave functions.

All first-principles calculations are performed using the Vienna *Ab initio* Simulation Package (VASP) [62] and the band structures are obtained from Wannier-interpolation band scheme using the WANNIER90 code [63,64]. K-point sampling for all calculations is Γ-centered Monkhorst-Pack [65] $12 \times 12 \times 12$. The kinetic energy cutoff is 450 eV and the lattice constant is kept at the experimental value. For the G_0W_0 and GW_0 calculations, total bands are 168, including 143 empty states.

The G_0W_0 and GW_0 calculated band structures of ordered $L2_1$ Ru_2TaAl are shown in Fig. 7. Both results indicate that Ru_2TaAl is a semimetal with a negative band gap (so-called pseudogap) of -0.36 and -0.38 eV from G_0W_0 and GW_0, respectively. In the vicinity of E_F, there are three hole degenerate pockets at the Γ point, compensated by one electron pocket centered at the X point. The hole pockets at Γ are dominated by the Ru $4d$ t_{2g} bands with a small admixture of Ta t_{2g} orbitals, while the electron pocket at the X is purely Ta $5d$ e_g orbitals. An overlap between hole and electron pockets crossing E_F gives rise to a semimetallic character for Ru_2TaAl. A similar result has been found from the calculations using the full-potential linearized augmented Slater-type orbital method [66]. It is remarkable that the size of the pseudogap obtained from each calculation is in satisfactory agreement with the value of 0.29 eV deduced from the ^{27}Al NMR $1/T_1$. On this basis, the activated behavior of $1/T_1$ at high temperatures could be reasonably realized as the thermal excitation of carriers across the pseudogap.

Figure 8 illustrates the calculated GW_0-PBE total and site-decomposed DOS of Ru_2TaAl. It is apparent that the total DOS spectrum consists of two peaks which are separated by a steep hybridization pseudogap centered at E_F with a residual Fermi-level DOS of 0.15 states/eV f.u. We also determined the Ta partial $5d$ DOS of 0.04–0.05 states/eV f.u. at E_F. In addition, the calculation reveals a small Al $3s$ Fermi-level DOS of about 0.004 states/eV f.u. which is consistent with 0.007 states/eV f.u. deduced from the analysis of the Korringa relation. With these accordances, it reinforces the conclusion that the G_0W_0 and GW_0 calculations using PBE initial wave functions give consistent results with good agreement with experimental observations. We thus conclude here that the inclusion of the many-body G_0W_0 and/or GW_0 effects is crucial to obtain correct band structures of the full Heusler compounds.

III. CONCLUSIONS

We have characterized the electronic properties of Ru_2TaAl by means of the transport, thermoelectric, specific heat, and NMR measurements. The semimetallic nature in Ru_2TaAl has been clearly evidenced by the observations of the thermally activated behavior, pointing out the existence of a pseudogap at around the Fermi level. First-principles total-energy calculations including G_0W_0 and GW_0 band corrections further indicate that the pseudogap arises from an indirect overlap between the electron and hole pockets, leading to a small Fermi-level DOS as observed. Moreover, we have demonstrated that the ZT value can be effectively enhanced through off-stoichiometric approach as found in the $Ru_{1.95}Ta_{1.05}Al$ compound. Namely, a substantial enhancement in the room-temperature ZT from Ru_2TaAl ($\sim 6.1 \times 10^{-4}$) to $Ru_{1.95}Ta_{1.05}Al$ ($\sim 3.4 \times 10^{-3}$) has been achieved. In this respect, a further improvement of thermoelectric performance in Ru_2TaAl through other attempts is highly probable and certainly warrants further investigations.

[1] C. Felser, L. Wollmann, S. Chadov, G. H. Fecher, and S. S. P. Parkin, APL Mater. **3**, 041518 (2015), and references therein.

[2] I. Galanakis, P. H. Dederichs, and N. Papanikolaou, Phys. Rev. B **66**, 174429 (2002).

[3] Y. Nishino, M. Kato, S. Asano, K. Soda, M. Hayasaki, and U. Mizutani, Phys. Rev. Lett. **79**, 1909 (1997).

[4] C.-S. Lue and J. H. Ross, Jr., Phys. Rev. B **58**, 9763 (1998).

[5] C. S. Lue, J. H. Ross, Jr., C. F. Chang, and H. D. Yang, Phys. Rev. B **60**, R13941(R) (1999).

[6] A. Ślebarski, M. B. Maple, E. J. Freeman, C. Sirvent, D. Tworuszka, M. Orzechowska, A. Wrona, A. Jezierski, S. Chiuzbaian, and M. Neumann, Phys. Rev. B **62**, 3296 (2000).

[7] C. S. Lue and J. H. Ross, Jr., Phys. Rev. B **63**, 054420 (2001).

[8] C. S. Lue, Y. Li, J. H. Ross, Jr., and G. M. Irwin, Phys. Rev. B **67**, 224425 (2003).

[9] A. Ślebarski and J. Goraus, Phys. Rev. B **80**, 235121 (2009).

[10] C. S. Lue, J. H. Ross, Jr., K. D. D. Rathnayaka, D. G. Naugle, S. Y. Wu, and W.-H. Li, J. Phys.: Condens. Matter **13**, 1585 (2001).

[11] A. Ślebarski, J. Deniszczyk, W. Borgieł, A. Jezierski, M. Swatek, A. Winiarska, M. B. Maple, and W. M. Yuhasz, Phys. Rev. B **69**, 155118 (2004).

[12] Y. Nishino, H. Kato, M. Kato, and U. Mizutani, Phys. Rev. B **63**, 233303 (2001).

[13] C. S. Lue and Y.-K. Kuo, Phys. Rev. B **66**, 085121 (2002).

[14] M. Vasundhara, V. Srinivas, and V. V. Rao, J. Phys.: Condens. Matter **17**, 6025 (2005).

[15] Y. Nishino, S. Deguchi, and U. Mizutani, Phys. Rev. B **74**, 115115 (2006).

[16] M. Vasundhara, V. Srinivas, and V. V. Rao, Phys. Rev. B **77**, 224415 (2008).

[17] M. Mikami, Y. Kinemuchi, K. Ozaki, Y. Terazawa, and T. Takeuchi, J. Appl. Phys. **111**, 093710 (2012).

[18] K. Renard, A. Mori, Y. Yamada, S. Tanaka, H. Miyazaki, and Y. Nishino, J. Appl. Phys. **115**, 033707 (2014).

[19] D. I. Bilc, G. Hautier, D. Waroquiers, G.-M. Rignanese, and P. Ghosez, Phys. Rev. Lett. **114**, 136601 (2015).

[20] H. Al-Yamani and B. Hamad, J. Electron. Mater. **45**, 1101 (2015).

[21] D. P. Rai, S. A. Shankar, R. Khenata, A. H. Reshak, C. E. Ekuma, R. K. Thapa, and S.-H. Ke, AIP Adv. **7**, 045118 (2017).

[22] Q. Feng, T. K. Nandy, and T. M. Pollock, Scr. Mater. **50**, 849 (2004).

[23] C. S. Lue and Y. K. Kuo, J. Appl. Phys. **96**, 2681 (2004).

[24] C. S. Lue, Y.-K. Kuo, S.-N. Horng, S. Y. Peng, and C. Cheng, Phys. Rev. B **71**, 064202 (2005).

[25] C. S. Lue, C. F. Chen, J. Y. Lin, Y. T. Yu, and Y. K. Kuo, Phys. Rev. B **75**, 064204 (2007).

[26] M. Yin and P. Nash, J. Alloys Compd. **634**, 70 (2015).

[27] T. Graf, C. Felser, and S. S. P. Parkin, Prog. Solid State Chem. **39**, 1 (2011).

[28] C. N. Kuo, H. W. Lee, C.-M. Wei, Y. H. Lin, Y. K. Kuo, and C. S. Lue, Phys. Rev. B **94**, 205116 (2016).

[29] Y. Hanada, R. O. Suzuki, and K. Ono, J. Alloys Compd. **329**, 63 (2001).

[30] T. Nakama, Y. Takaesu, K. Yagasaki, T. Naka, A. Matsushita, K. Fukuda, and Y. Yamada, J. Phys. Soc. Jpn. **74**, 1378 (2005).

[31] H. Okamura, J. Kawahara, T. Nanba, S. Kimura, K. Soda, U. Mizutani, Y. Nishino, M. Kato, I. Shimoyama, H. Miura, K. Fukui, K. Nakagawa, H. Nakagawa, and T. Kinoshita, Phys. Rev. Lett. **84**, 3674 (2000).

[32] I. Maksimov, D. Baabe, H. H. Klauss, F. J. Litterst, R. Feyerherm, D. M. Többens, A. Matsushita, and S. Süllow, J. Phys.: Condens. Matter **13**, 5487 (2001).

[33] A. Matsushita, T. Naka, Y. Takano, T. Takeuchi, T. Shishido, and Y. Yamada, Phys. Rev. B **65**, 075204 (2002).

[34] K. Soda, H. Murayama, K. Shimba, S. Yagi, J. Yuhara, T. Takeuchi, U. Mizutani, H. Sumi, M. Kato, H. Kato, Y. Nishino, A. Sekiyama, S. Suga, T. Matsushita, and Y. Saitoh, Phys. Rev. B **71**, 245112 (2005).

[35] V. N. Antonov, A. Ernst, I. V. Maznichenko, A. N. Yaresko, and A. P. Shpak, Phys. Rev. B **77**, 134444 (2008).

[36] D. I. Bilc and P. Ghosez, Phys. Rev. B **83**, 205204 (2011).

[37] D. Do, M.-S. Lee, and S. D. Mahanti, Phys. Rev. B **84**, 125104 (2011).

[38] C. S. Lue, M. D. Chou, N. Kaurav, Y. T. Chung, and Y. K. Kuo, Appl. Phys. Lett. **94**, 192105 (2009).

[39] C. S. Lue, Y. S. Tseng, J. Y. Huang, H. L. Hsieh, H. Y. Liao, and Y. K. Kuo, AIP Adv. **3**, 072132 (2013).

[40] Y.-K. Kuo, B. Ramachandran, and C.-S. Lue, Front. Chem. **2**, 106 (2014).

[41] C. Wan, Y. Wang, N. Wang, W. Norimatsu, M. Kusunoki, and K. Koumoto, Sci. Technol. Adv. Mater. **11**, 044306 (2010).

[42] C. S. Lue, W. J. Lai, C. C. Chen, and Y.-K. Kuo, J. Phys.: Condens. Matter **16**, 4283 (2004).

[43] C. S. Lue, J. W. Huang, D. S. Tsai, K. M. Sivakumar, and Y.-K. Kuo, J. Phys.: Condens. Matter **20**, 255233 (2008).

[44] I. Knapp, B. Budinska, D. Milosavljevic, P. Heinrich, S. Khmelevskyi, R. Moser, R. Podloucky, P. Prenninger, and E. Bauer, Phys. Rev. B **96**, 045204 (2017).

[45] F. S. da Rocha, G. L. F. Fraga, D. E. Brandão, C. M. da Silva, and A. A. Gomes, Physica B **269**, 154 (1999).

[46] J. Winterlik, G. H. Fecher, C. Felser, M. Jourdan, K. Grube, F. Hardy, H. von Lohneysen, K. L. Holman, and R. J. Cava, Phys. Rev. B **78**, 184506 (2008).

[47] C. S. Lue, S. M. Huang, C. N. Kuo, F.-T. Huang, and M.-W. Chu, New J. Phys. **10**, 083029 (2008).

[48] C. S. Lue and S. C. Chen, Phys. Rev. B **79**, 125108 (2009).

[49] J. Korringa, Physica **16**, 601 (1950).

[50] C. S. Lue, S. Y. Wang, and C. P. Fang, Phys. Rev. B **75**, 235111 (2007).

[51] C. P. Fang, C. S. Lue, and B.-L. Young, Phys. Rev. B **83**, 113105 (2011).

[52] E. A. Hill, P. Volkov, S. J. Poon, and Y. Wu, Phys. Rev. B **51**, 4865 (1995).

[53] C.-S. Lue, S. Chepin, J. Chepin, and J. H. Ross, Jr., Phys. Rev. B **57**, 7010 (1998).

[54] C. S. Lue, B. X. Xie, S. N. Horng, J. H. Su, and J. Y. Lin, Phys. Rev. B **71**, 195104 (2005).

[55] C. S. Lue, J. Y. Lin, and B. X. Xie, Phys. Rev. B **73**, 035125 (2006).

[56] C. S. Lue, B. X. Xie, and C. P. Fang, Phys. Rev. B **74**, 014505 (2006).

[57] M. S. Hybertsen and S. G. Louie, Phys. Rev. B **34**, 5390 (1986).

[58] J. P. Perdew, K. Burke, and M. Ernzerhof, Phys. Rev. Lett. **77**, 3865 (1996).

[59] A. V. Krukau, O. A. Vydrov, A. F. Izmaylov, and G. E. Scuseria, J. Chem. Phys. **125**, 224106 (2006).

[60] M. Shishkin and G. Kresse, Phys. Rev. B **75**, 235102 (2007).
[61] M. Shishkin and G. Kresse, Phys. Rev. B **74**, 035101 (2006).
[62] G. Kresse and J. Furthmüller, Phys. Rev. B **54**, 11169 (1996).
[63] A. A. Mostofi, J. R. Yates, Y.-S. Lee, I. Souza, D. Vanderbilt, and N. Marzari, Comput. Phys. Commun. **178**, 685 (2008).
[64] D. R. Hamann and D. Vanderbilt, Phys. Rev. B **79**, 045109 (2009).
[65] H. J. Monkhorst and J. D. Pack, Phys. Rev. B **13**, 5188 (1976).
[66] M. Weinert and R. E. Watson, Phys. Rev. B **58**, 9732 (1998).